crystals

MDPI

Review

Formation of Metastable Crystals from Supercooled, Supersaturated, and Supercompressed Liquids: Role of Crystal-Liquid Interfacial Free Energy

Geun Woo Lee [1,2]

[1] Korea Research Institute of Standards and Science, Daejon 305-340, Korea; gwlee@kriss.re.kr
[2] Department of Nano Science, University of Science and Technology, Daejeon 305-333, Korea

Academic Editor: Helmut Cölfen
Received: 28 July 2017; Accepted: 26 October 2017; Published: 29 October 2017

Abstract: The formation mechanism of metastable crystals from metastable liquids still remains elusive, although controlling the metastability of crystals and liquids already plays a crucial role in designing new materials in physics, chemistry, biology, and materials science. This review article describes how metastable phases can be obtained by controlling temperature, concentration, and pressure. In particular, I show the role of crystal-liquid interfacial free energy in the formation of metastable crystals from metastable liquids at a given driving force. In a microscopic viewpoint, local structure similarity between the metastable crystals and liquid determines the crystal-liquid interfacial free energy, and thus the nucleation barrier for the metastable crystals. The effect of the interfacial free energy on the formation of metastable crystals from supercooled, supersaturated, and supercompressed liquids will be demonstrated with metallic liquids, aqueous solutions, and water.

Keywords: metastable crystals; metastable liquids; crystal-liquid interfacial free energy; local orders; nucleation; supercooling; supersaturation

1. Introduction

Metastable liquids are defined as liquids that are placed out of equilibrium states, such as a supercooled state below equilibrium melting temperatures, a supersaturated state above saturated concentration, or a supercompressed state beyond equilibrium melting pressures. Those liquids eventually transform into other stable or metastable phases at a given temperature, concentration, and pressure. Over a century ago, Ostwald [1] recognized that an initial crystal phase nucleated from a metastable liquid could often be one of the intermediate phases, rather than the most thermodynamically stable phase. Theoretically, Santen [2] suggested a theoretical model to understand this phenomenon; such a process of taking intermediate phases for crystallization minimizes entropy production for the transformation. It implies that the transformation results from the entropic similarity (or similarity of local orders) between liquid and crystals during each transformation step. Furthermore, it implies that there are multiple pathways of nucleation [3] (e.g., aqueous [4] and mineral [5,6] solutions, alloy liquids [7,8], pure water [9,10], and even crystals [11], and so on) forming metastable phases. For instance, crystallization in deeply supercooled liquids can be mainly governed by nucleation and growth processes, or spinodal decomposition [12]. While the former requires overcoming an energy barrier for a transition given by thermodynamics, the latter does not. This depends whether, for example, the supercooled liquids are in a metastable or unstable state. In this work, we focus on the former case to understand the detailed formation mechanism of metastable crystals from the metastable liquids that are manifested via supercooling, supersaturating, and supercompressing. In particular, we discuss the effect of crystal-liquid interfacial free energy on the formation of metastable crystals.

In case of supercooled metallic liquids, an example of the metastable liquids, Turnbull [13] demonstrated the astonishing stability of liquid metals, as most liquid metals can be supercooled to around 20% below their equilibrium melting temperatures without crystallization. Microcrystalline models [14], which were widely accepted at that time, had an expected small crystal-liquid interfacial free energy and nucleation barrier, since the model described crystal fragment as a liquid structure. Therefore, the model was inadequate for explaining the deep supercooling phenomenon. Ultimately, the observation of such deep undercooling had required alternate insights for crystal-liquid interface and local structure of liquids. The first explanation for the local structure of the liquid metals was provided by Frank in 1952 [15]. He suggested an icosahedral short range order (ISRO) as the local order of the liquid metals. The ISRO having higher packing density (0.836) and lower energy (8.4%), with greater isotropic potential than the local order of closed packing crystal phases could account for the stability of the supercooled liquid. Furthermore, the ISRO lacks periodicity, naturally producing a disordered nature in the liquid metals, which causes high crystal-liquid interfacial free energy.

The detailed description of the relation between short range order and crystal-liquid interfacial free energy was given by Spaepen; the origin of the interfacial free energy is due to the configurational entropy difference (i.e., similarity of local orders) between crystal and liquid [16–18]. This model expected large amount of supercooling, if the local order of the crystal differed a lot from that of the liquids. On the contrary, the model predicts that the melt of quasicrystals can easily crystallize, since both liquid and crystal phases have same ISRO. This has been indirectly observed in the formation of metastable icosahedral quasicrystal formation from glass, which is a frozen supercooled liquid [19,20]. The prediction by Frank and Spaepen, i.e., the correlation of ISRO and interfacial free energy, were directly vindicated by the aid of new technical development over a last decade. That is a combination of levitations and scattering techniques [4,7,8,21–23] providing containerless environment that suppresses heterogeneous nucleation sites, makes easy deep supercooling, and gives more accurate diffraction signal.

Using the combined techniques, the interfacial free energy and SROs of supercooled liquids have been reported with elemental metals (Ti [22–24], Fe [25–27], Ni [23,27,28], Zr [28,29]) and many alloys [7,8,21,29–33]. Particularly, a combination of electrostatic levitation (ESL) and X-ray synchrotron scattering revealed for the first time the relationship between SRO and nucleation barriers with Ti-Zr-Ni alloy liquids [17]. That is, the liquids showed different degree of supercooling depending on the SRO of crystal phases [7,8,21,23,28,29]. This finding is indeed consistent with Spaepen's model. In addition, $Ti_xZr_{(79-x)}Ni_{21}$ (x = 33~45 at.%) liquids primarily transformed into a metastable icosahedral quasicrystal phase (i-phase), even with small undercooling, rather than a competing stable C14 Laves phase [7,8,21] with large amounts of undercooling. The formation of the i-phase reflects a smaller interfacial free energy for the i-phase than for the C14 Laves phase, which overwhelms the smaller driving force for the i-phase. Furthermore, it was recently reported that an extended ISRO or icosahedral medium range order (IMRO) could significantly reduce the quasicrystal-liquid interfacial free energy and stabilize a metastable i-phase [8,32].

The relation between SRO and crystal-liquid interfacial free energy can be extended to crystallization in aqueous solution. Recently, we have developed a novel ESL technique by combining real-time micro-Raman and X-ray scattering for the first time [4,34]. The method enables the achievement of a degree of supersaturation, which has never been demonstrated by conventional methods, by probing the atomic and molecular structures of the supersaturated solutions. In particular, when a levitated KH_2PO_4 (KDP) solution reaches extremely high supersaturation, surprisingly, the supersaturated solution transforms into a metastable KDP crystal phase (monoclinic) rather than a stable phase (tetragonal) at room temperature [4]. We find that this phenomenon is influenced by a smaller interfacial free energy between the metastable solution and the metastable crystal, rather than the stable crystal.

A metastable liquid can be also formed by controlling pressure. Liquid water contains many metastable crystals [35–37] and amorphous phases [38–40] under high pressure and at low

temperature conditions. If we can minimize mechanical perturbation to water during compression, the water can be highly supercompressed, and transforms into other metastable phases at room temperature (e.g., ice VII and amorphous). This was demonstrated by a dynamic diamond anvil cell (dDAC) technique which can control compression rate [9,10,41]. The transformation was also understood in terms of similarity of local orders between the metastable ice VII phases and the supercompressed water, which results in a lower interfacial free energy for the metastable phase as compared to the stable crystal ice VI [9].

In this present, we review the formation of metastable crystals from supercooled, supersaturated, and supercompressed liquids. Afterwards, we briefly cover classical nucleation theory, in which means that the estimation of the interfacial free energy and its connection to local orders are elaborated upon. Finally we discuss the effect of crystal-liquid interfacial free energy and local orders of liquids on the stability of metastable liquids, such as metallic liquids, aqueous KH_2PO_4 solution, and liquid water (H_2O).

1.1. Classical Nucleation Theory: Estimation of Crystal-Liquid Interfacial Free Energy

First, we briefly review the classical nucleation theory and make a connection of crystal-liquid interfacial free energy to local structural similarity. According to the classical homogeneous nucleation theory (CNT), crystal nuclei are formed through stochastic fluctuation of atomic clusters (i.e., density fluctuation) in a metastable liquid. The stability of a crystal nucleus (or a cluster) in the liquid is governed by volume Gibbs free energy ($\Delta G_v = G^l - G^c$, the difference of Gibbs free energy of liquid (G^l) and crystal (G^c)) and crystal–liquid interfacial free energy (σ), that is, $\Delta G_n = (4/3)\pi r^3 \Delta G_v + 4\pi r^2 \sigma$, where r is the radius of the nucleus. Once the liquid cools down to below its melting temperature, the probability of nuclei formation increases due to increasing driving force. If the size of the nuclei formed in the supercooled liquid is larger than a critical size, $r^* = 2\sigma/(\Delta G_v)$, the nuclei starts growing. At a given supercooled temperature, if at least one critical nucleus is to initiate crystallization, the product of nucleation rate, sample volume, and elapsed time is required to be greater than one (that is, its multiplication gives the number of nuclei):

$$\int_0^{\mathrm{t}} \mathrm{I^s(T)V(T)dt'} = \sum_{\mathrm{t=0}}^{\mathrm{t=\tau}} \mathrm{I^s(T) \times V(T) \times t} \geq 1 \tag{1}$$

where time $t = 0$ refers to the onset of the supercooling, and time $t = \tau$ means the onset of nucleation. The steady state nucleation rate I^s, the number of nuclei per unit time per unit volume at a given temperature T, is given by a reference [42]:

$$I^s = \frac{6n^{*2/3} k_B T N_A}{\pi \eta(\mathrm{T}) \lambda^3} \left(\frac{|\delta\mu|}{6\pi k_B T n*} \right)^{1/2} \exp\left(-\frac{\Delta G_n*}{k_B T} \right) \tag{2}$$

where, η, λ, n^* ($= \frac{32\pi v_m^2 \sigma^3}{3(\delta\mu)^3}$), $\delta\mu$, k_B, N_A, and $\Delta G_n{}^*$ are viscosity, average atomic jump distance, the number of atoms in the critical nucleus, the volume Gibbs free energy difference per atoms between initial and final phases, the Boltzmann's constant, the Avogadro number, and the work (i.e., nucleation barrier) of critical cluster formation, respectively. The work (or energy barrier for nucleation) $\Delta G_n{}^*$ is determined by the $\delta\mu$, the interfacial free energy σ, and the average atomic volume v:

$$\Delta G_n* = \frac{16\pi}{3} \frac{\sigma^3}{(\delta\mu/\mathrm{V})^2} \tag{3}$$

The volume of the Gibbs free energy difference per atoms has been proposed with many different forms, depending on the materials. Here, we use three different Gibbs free energies (Turnbull [43], Thompson and Spaepen [44], Sigh and Holz [45]) between liquid and crystal:

$$\delta\mu = \Delta G_v / N_A = \frac{\Delta H_f \Delta T}{T_m} \text{ (Turnbull)} \quad (4)$$

$$\delta\mu = \frac{\Delta H_f \Delta T}{T_m} \frac{2T}{T_m + T} \text{ (Thompson and Spaepen)} \quad (5)$$

$$\delta\mu = \frac{\Delta H_f \Delta T}{T_m} \frac{7T}{T_m + 6T} \text{ (Sigh and Holz)} \quad (6)$$

Here, ΔH_f, ΔT, and T_m are fusion enthalpy, the amount of supercooling, and melting temperature, respectively. In case of supersaturation and supercompression, the driving force are given by $\delta\mu = k_B\ T\ \ln s$, and $\delta\mu = \Delta V^{l\text{-}s}\ \Delta P$, respectively, where s is supersaturation, $\Delta V^{l\text{-}s}$ is the volume difference of the crystal and liquid, and ΔP is the over-pressured value. The degree of supersaturation is defined as $s = C_s/C_e$, where C_s and C_e are sample concentration and saturation concentration, respectively. When the thermophysical parameters in Equations (2)–(5) are given, the interfacial free energy satisfying the Equation (1) can be estimated. Note that Equations (1)–(6) require homogeneous nucleation, supercooling, and the thermophysical parameters (e.g., melting temperature, supercooled temperature, fusion enthalpy, density or volume, viscosity, and time). The requirement can be achieved by ESL, which is depicted in details [46].

A connection between local order and thermodynamic properties of interfacial free energy is given by Spaepen's model [16–18]; the different local orders (i.e., configurational entropy difference) of crystal and liquid underlies crystal-liquid interfacial free energy, which is given by:

$$\alpha_r = \frac{\sigma}{\Delta H_f} = \frac{N_i}{N}\left(\frac{\Delta S_{config}(\text{Bulk}) - \Delta S_{config}(\text{Interface})}{\Delta S_f}\right) \quad (7)$$

where α is called Turnbull's coefficient, i.e., interfacial free energy (σ) per fusion enthalpy per atom (ΔH_f), N_i is the number of atoms in the interface, N is the number of atoms in the crystal plane, ΔS_{config}(Bulk) is the configurational entropy of the bulk crystal, ΔS_{config}(Interface) is the configurational entropy of the interface, and ΔS_f is the fusion entropy per atom. Therefore, from Equation (1), one expects a large interfacial free energy, if local orders (or SROs) between the liquid and crystal are significantly different, causing a large configurational entropy difference between the two phases.

1.2. Formation of a Metastable Crystal from a Metastable Liquid

Figure 1a shows a schematic diagram of volume Gibbs free energies of liquid, crystal, and metastable crystal. While the Gibbs free energy of a liquid is lower than that of the crystals above its melting temperature $T_m{}^s$, the Gibbs free energy of the stable crystal is lower than the other two phases below melting temperature. This gives rise to a higher driving force $\Delta G_v{}^{l\text{-}s}$ for the stable crystal, than $\Delta G_v{}^{l\text{-}ms}$ for the metastable crystal, which inhibits formation of the metastable crystal in the supercooled liquid. Nevertheless, if the metastable crystal forms, it implies that the work required for the nucleation of the metastable crystal is less than for stable crystal, i.e., $(\Delta G_n{}^* \sim \sigma^3/\delta\mu^2)_{ms} < (\Delta G_n{}^*)_s$. This indicates that the interfacial free energy for the metastable crystal is smaller than that of the stable one, which compensates the smaller driving force for the metastable crystal in Figure 1a. Such a case is depicted in Figure 1b; upon supercooling above C′, the supercooled liquid transforms into the stable crystal following crystallization path A′, as shown in Figure 1c. However, at supercooling marked by B′, a nucleation barrier for the metastable crystal is smaller than that of the stable crystal, although the amount of undercooling $\Delta T^{ms} = T^{ms}{}_m - T_{B'}$ for metastable crystal is smaller than $\Delta T^s = T^s{}_s - T_{B'}$ for stable crystal. Therefore, the liquid temperature rises to the melting temperature of the metastable crystal, due to the release of latent heat. We can often perceive a step recalescence as a signal for the formation of the metastable crystal, which follows path B′ in Figure 1c. Accordingly, the formation of the metastable phase depends on the competition between interfacial

free energy and driving force. We note that the step behavior upon recalescence does not always imply the formation of metastable crystals.

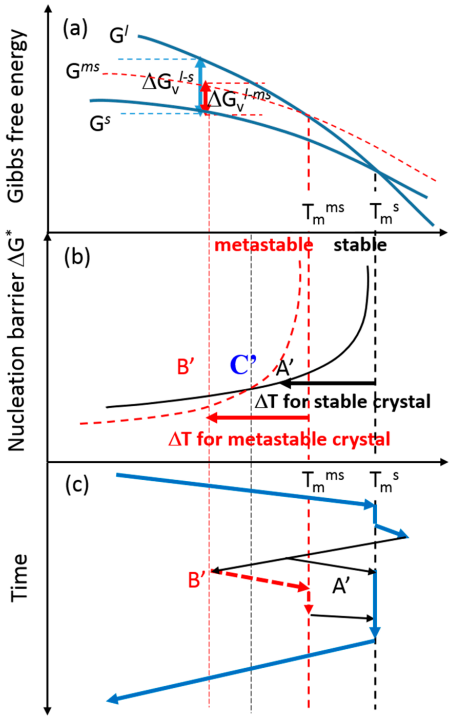

Figure 1. Schematic figures for Gibbs free energy of liquid, metastable and stable crystal phases (**a**), nucleation barrier (**b**), and melting and crystallization path (**c**) depending on undercooling in (**b**).

2. Results and Discussion

2.1. Metastable Icosahedral Quasicrystal Formation from Supercooled Ti-Zr-Ni Alloy Liquids

Ti-Zr-Ni alloys are one of the best materials for studying the relationship between crystal–liquid interfacial free energy and SRO as a function of crystal SRO, since the alloys show various crystal phases, such as simple crystalline, complex polytetrahedral crystalline, and icosahedral quasicrystalline phases [7,8,21,47]. Figure 2a shows a double-step recalescence from a supercooled Ti-Zr-Ni liquid. Upon crystallization, the temperature rises up to around 790 °C due to the release of latent heat. This event corresponds to the formation of a metastable icosahedral quasicrystal (i-phase). The i-phase subsequently transforms into the stable C14 Laves phase (hcp structure) with a second temperature rise at around 810~820 °C, based on the phase diagram [7,8,21,47]. Both phase formations were directly confirmed by in situ real-time X-ray scattering [7]. The temperature rising is exactly same feature with marked B′ path in Figure 1c. Therefore, the plateau temperature of ~785 °C indicates the melting of the i-phase. This is the experimental example shown in Figure 1b,c. More specifically, the supercooled liquid at 780 °C transforms directly into the formation of the stable C14 Laves phase, while the liquid at 760 °C forms a metastable i-phase (Figure 2c,d). Since the melting temperatures of each phase are 820 °C and 785 °C respectively, the amount of undercooling (ΔT) for i-phase at 760 °C is about 25 °C, while ΔT for Laves phase at 780 °C is about 30–40 °C. This result implies a smaller driving force was needed for i-phase formation. Therefore, the smaller nucleation barrier for the i-phase is attributed to the smaller interfacial free energy.

The relation between interfacial free energy and the SROs of the supercooled Ti-Zr-Ni liquids and crystals has been reported [7,8,29,30]. All Ti-Zr-Ni liquids showed an ISRO which was measured by scattering experiments [7,29]. Simple crystalline phases of elemental transition metals and alloy liquids

with bcc structure [21,24–27] showed the highest undercooling ($\Delta T_r = (T - T_r)/T_l = 0.18$, where T_r and T_l is recalescence and liquidus temperatures, respectively) and interfacial energy ($\sigma(J/m^2)$) per fusion enthalpy (ΔH_f) (i.e., Turnbull coefficient α (= $\sigma/\Delta H_f$ = 0.39~0.61)), compared with other crystal phases. For icosahedral quasicrystalline phases (i-phase), the lowest undercooling and α were obtained with 0.1 and 0.32~0.34, respectively [7,8,21]. A Laves phase with the hcp structure in a large unit cell, but ISRO in short range yields intermediate values of undercooling (0.14) and α (0.37~0.43) [7,8,21]. The smallest interfacial free energy indeed resulted from the similarity in local orders, since both i-phase and its liquid have ISRO, as we discussed in Equation (6). We have also found an opposite example in Cu-Zr bulk metallic glasses (BMG). The $Cu_{64}Zr_{36}$ alloy shows deeper undercooling and the longer persistent time at supercooled temperatures than neighboring compositions, indicating a high glass forming ability (GFA) with high nucleation barrier [48]. This finding reflects a higher interfacial free energy at a certain normalized temperature, due to relatively less similarity of local orders between the liquid and crystal. A recent simulation result showed that an increasing contribution of five-fold symmetry in liquid, leading to an increase in crystal–liquid interfacial free energies, which consequently suppressed the formation of crystal nucleation [49,50].

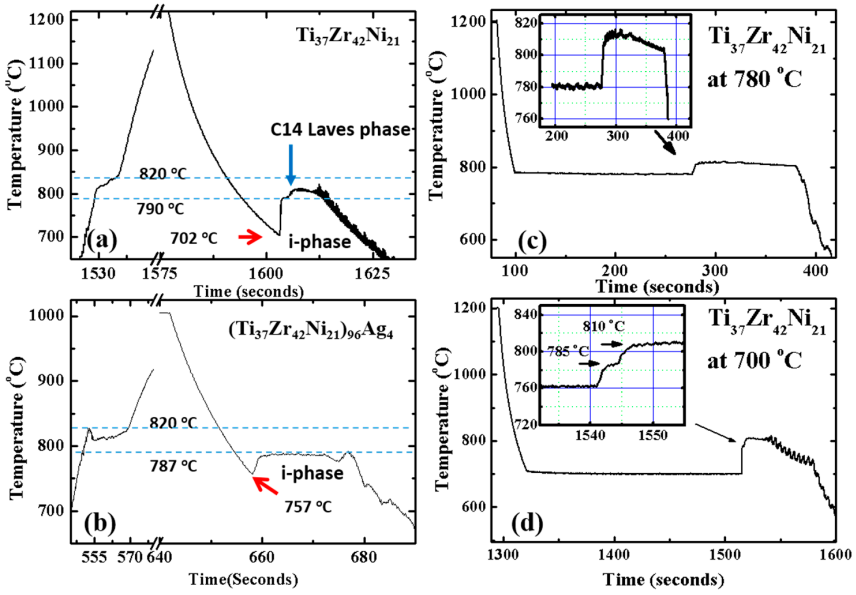

Figure 2. Temperature-time (T-t) curves measured in electrostatic levitation (ESL). A typical T-t curve forming metastable i-phase and C14 Laves phase (hcp structure) on $Ti_{37}Zr_{42}Ni_{21}$ alloy (**a**) [8]; A typical T-t curve forming i-phase only on $(Ti_{37}Zr_{42}Ni_{21})_{96}Ag_4$ alloy (**b**) [8]; The formation of stable C14 Laves phase from undercooled liquid at 780 °C (**c**) [21]; The formation of metastable i-phase and stable C14 Laves phase at 760 °C (**d**) [21].

Furthermore, provided that the ISRO develops in the liquid, the i-phase can be formed much more effectively. As an example, it is known that small amount of Ag addition to as-casted Ti-Zr-Ni alloys yields improved thermal stability and longer coherence length for crystallinity of the i-phase [32]. Undercooling behavior shown in Figure 2b follows the behaviors of the as-casted alloys. That is, the liquid with small Ag addition only transforms into i-phase with a small amount of undercooling. According to CNT, the small amount of undercooling requires a large size of critical nuclei, which usually hinders nucleation. Nevertheless, the formation of the i-phase from the small amount of undercooling (Figure 2b) implies that the addition of Ag facilitates formation of nuclei with larger critical sizes. Moreover, the long plateau time and absence of the C14 Laves phase in Figure 2b reflect that the i-phase is more stabilized with the addition of Ag. These observations (i.e., enhanced thermal stability and large size of nuclei) indicate the addition of Ag led to development

of ISRO in the supercooled liquid. Recent studies reported that quasicrystal growth was facilitated by structurally persistent atoms that were kinetically trapped in icosahedral clusters nearby the quasicrystal nucleus [48,49], which reflected the existence of a structural correlation which is longer than SRO, i.e., icosahedral medium range order (IMRO). Indeed, the IMRO in the Ti-Zr-Ni-Ag alloy was observed in an ab initio molecular simulation study that showed a global structural ordering by Zr-Ag pairs [8]; ratios of peak positions (R_n) to the first peak (R_1) of Zr-Ag pair distribution function were close to the ideal values [51], i.e., $\frac{R_2}{R_1} = \sqrt{3}$, $\frac{R_3}{R_1} = \sqrt{4}$, $\frac{R_4}{R_1} = \sqrt{7}$, and $\frac{R_5}{R_1} = \sqrt{12}$. Therefore, the formation of IMRO on the Ti-Zr-Ni liquid enhances the similarity of local structure between i-phase and its liquid, resulting in a small interfacial free energy, and thus a lower nucleation barrier for the formation of the icosahedral quasicrystal with Ag addition, as shown in Table 1. It should be noted that all of the interfacial free energies in $(Ti_{37}Zr_{42}Ni_{21})_{96}Ag_4$ are smaller than in the $Ti_{37}Zr_{42}Ni_{21}$ alloy, regardless of driving force. One can predict that extremely small undercooling or no supercooling, if a liquid has extended local ordering that is very similar to that of crystals, percolates throughout the liquid, and becomes sufficiently dominant in the liquid with high population, even above liquidus temperature. This concept may blur the distinction between homogeneous and heterogeneous nucleation in classical nucleation theory. On the other hand, if the extended local ordering of the liquid differs from that of the crystal, the liquid can deeply supercool and become glass.

Table 1. A degree of supercooling, interfacial free energy, Turnbull coefficient, nucleation barrier, critical nuclei radius of $Ti_{37}Zr_{42}Ni_{21}$ and $(Ti_{37}Zr_{42}Ni_{21})_{96}Ag_4$ alloys [8].

Compositions & Used Parameters (T_l, ϱ, C_p, ΔH_f)	$\Delta T/T_m$	Interfacial Energy (σ) (±0.0002)			α (=σ/ΔH_f)	W*/k_BT at T_r	r*(I) (nm)	Coherence Length (nm) on as Cast i-Phase
		$\Delta G_{l\text{-}s}(1)$	$\Delta G_{l\text{-}s}(2)$	$\Delta G_{l\text{-}s}(3)$				
$Ti_{37}Zr_{42}Ni_{21}$ (T_l = 1060 K, ϱ = 5.95 g/cm^3, C_p = 44.24 J/mol-K, ΔH_f = 8.1 kJ/mol)	0.1	0.061	0.049	0.050	0.324	665.17	1.735	25
$(Ti_{37}Zr_{42}Ni_{21})_{96}Ag_4$ (T_l = 1060 K, ϱ = 5.98 g/cm^3, C_p = 44.24 J/mol-K, ΔH_f = 7.93 kJ/mol)	0.029	0.027	0.022	0.022	0.146	58.84	2.736	43

$\Delta G_{l-s}(1) = \frac{\Delta T \Delta H_f}{T_i}$, $\Delta G_{l-s}(2) = \frac{\Delta T \Delta H_f}{T_m} \frac{2T}{T_l + T}$, $\Delta G_{l-s}(3) = \frac{\Delta T \Delta H_f}{T_m} - \gamma \Delta S_f (\Delta T - T \ln(\frac{T_l}{T}))$.

2.2. Metastable Monoclinic KH_2PO_4 (KDP) Crystal Formation From A Supersaturated KDP Solution

A metastable state of liquids can be achieved by supersaturating aqueous solutions. We have, for the first time, developed an apparatus that combines ESL with real-time micro-Raman and X-ray scattering to probe atomic and molecular structures of supersaturated solutions as well as relevant thermophysical properties [4,34]. Containerless environments provided by the apparatus suppresses potential heterogeneous nucleation sites, enabling the KDP solution to be extremely supersaturated above s = 4 by evaporation at room temperature as shown in Figure 3a. We note that, in conventional method with a container, the level of supersaturation has never exceeded over s = 2 for KDP solution. To our surprise, after performing the supersaturation experiments more than 130 times, we discovered that the KDP solution carries two distinctive crystallization tendencies (See Figure 3b).

Based on CNT, the decreasing nucleation rate ((I) in Figure 3b) may result from changes in viscosity that increases with supersaturation (see Equation (2)). Therefore, the second crystallization event, which occurs beyond s = 3 in Figure 3b, is an indication of another type of nucleation events. Based on in situ real-time X-ray scattering experiments, we have identified both crystallization events; tetragonal KDP crystal forms in the solution with relatively low level of supersaturation (below s = 3 as marked by (I) in Figure 3b,c). The second-type nucleation event, which occurs when the supersaturation is greater than s = 3 (marked by (II) in Figure 3b,c), leads to the formation of monoclinic KDP crystal at room temperature. Approximately 40 min to an hour following the initial crystal nucleation, the monoclinic KDP crystal makes a secondary transformation into a tetragonal

crystal. The result clearly reflects that the monoclinic crystal is a metastable phase (See upper panel in Figure 3c). In situ real-time micro-Raman scattering experiments showed consistent results [4].

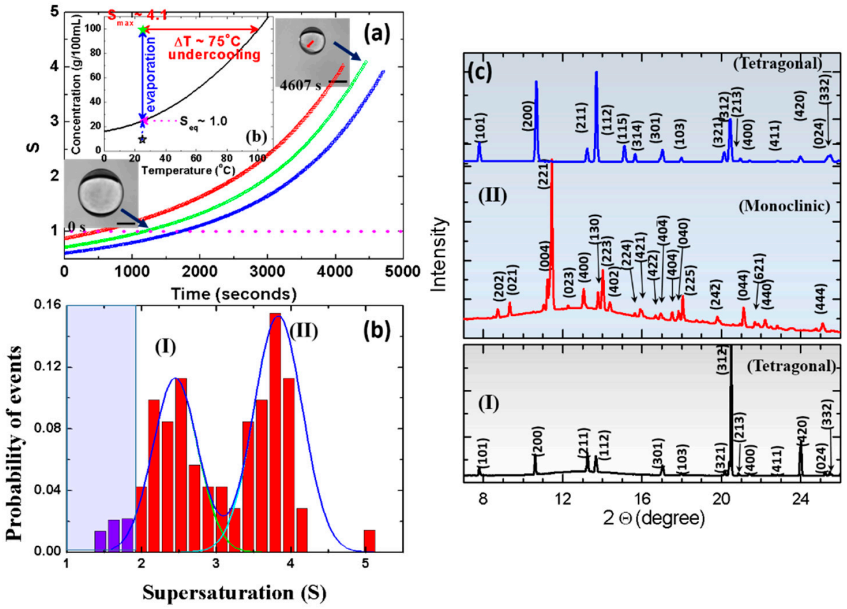

Figure 3. Increasing degree of supersaturation of the KH_2PO_4 (KDP) solution with time by evaporation process at room temperature (**a**) [4]; The saturation curves represent experimental trials that were performed with different initial concentrations (blue, 15 g/100 mL; green, 18 g/100 mL; red, 22 g/100 mL). Inset figure shows the state of metastability of the KDP droplet at s = 4.1 is equivalent to undercooling from 100 °C. The scale bar in the droplet images is 1 mm. Probability of crystallization events with supersaturation (**b**) [4]; Formation of stable (I) and metastable (II) phases of the KDP crystal from the supersaturated solution depends on the supersaturation, in which crystallizations took place (**c**) [4]. As shown in the upper panel of (II) in figure (**c**), the monoclinic KDP phases finally transforms into the stable tetragonal KDP crystal after 30 min to 1 h during the levitation, which indicates that the monoclinic KDP is metastable. The diffraction intensity difference of tetragonal phases in figure (**c**) resulted from directional crystal growth at the initial stage of the crystallization (I).

The estimated interfacial free energy for the stable KDP crystal at s = 3 is 34.5 mJ/m^2 based on Equation (2). This value is significantly greater than any other results previously reported [52–59] (i.e. σ = 2~16.87 mJ/m^2 for s = 1.2~1.95). Although it is non-trivial to determine the solubility curve for the metastable crystal (monoclinic phase), its metastable zone should be higher than s = 1, a lower limit for the stable crystal (tetragonal). Based on the Gaussian fit to the second crystallization event (II), we estimate that the saturation regime for the metastable phase may lie around s = 2.6. In any case, the driving Gibbs free energy or chemical potential ($\delta\mu = kT\ ln\ s$) for the stable phase is greater than the metastable phase. Therefore, the formation of metastable KDP means that the interfacial energy of the metastable phase should be smaller than that of the stable phase, i.e., $\sigma_{ms}{}^3 < \sigma_s{}^3\ (ln\ s_{ms}/ln s_s)^2$, where subscripts *ms* and *s* denote metastable and stable phases) since the nucleation barrier is given by $\Delta G^* (\sim\sigma^3/(ln\ s)^2)$.

Based on Equation (7), the formation of the metastable phase implies the configurational similarity of local structures between the solution and the metastable crystal. Raman scattering revealed a precursor that the tetrahedral order of H_2PO_4 in the KDP solution changes with supersaturation. X-ray scattering showed four different distorted tetrahedral for the metastable KDP crystal [4]. Therefore, one can expect that the highly concentrated solution carries local structural order that resembles that of the metastable KDP crystal. Further study is needed to prove the similarity of monoclinic ordering in liquid and crystal.

2.3. Formation of Metastable Ice VII Crystal And High Density Amorphous From Supercompressed Water

A metastable liquid phase can be obtained by over-pressurizing the liquid above its melting pressure where a crystal phase exists. Ideally, if there is no mechanical perturbation, which can trigger nucleation in the liquid, the liquid can be supercompressed. Experimentally, we have achieved the supercompressed liquid by using a dynamic diamond anvil cell (dDAC) technique, in which piezo-actuators drive the compressive motion as well as its rate [9,41,60]. For instance, we have supercompressed liquid water with varying compression rate using dDAC. With a slow compression rate (0.08 GPa/s), the water can be compressed well beyond its melting pressure of 0.9 GPa up to 1.2 GPa before finally crystallizing to an ice VI phase (See Figure 4a). On decompression, the ice VI phase transforms into water at 0.9 GPa. However, this crystallization path can be altered by applying a different compression rate. When a faster compression rate of 0.16 GPa/s was applied, the water was supercompressed to up to 1.8 GPa. Subsequently, the highly supercompressed water transforms into a metastable ice VII phase at 1.8 GPa, a pressure region for the VI phase field (Figure 4b,c). Recent study showed that the metastable ice VII phase immediately transformed into high density amorphous ice (HDA) phase within 50 μs [10]. On decompression, the HDA transforms into ice VI, and then melts subsequently with two main melting plateaus [9,10].

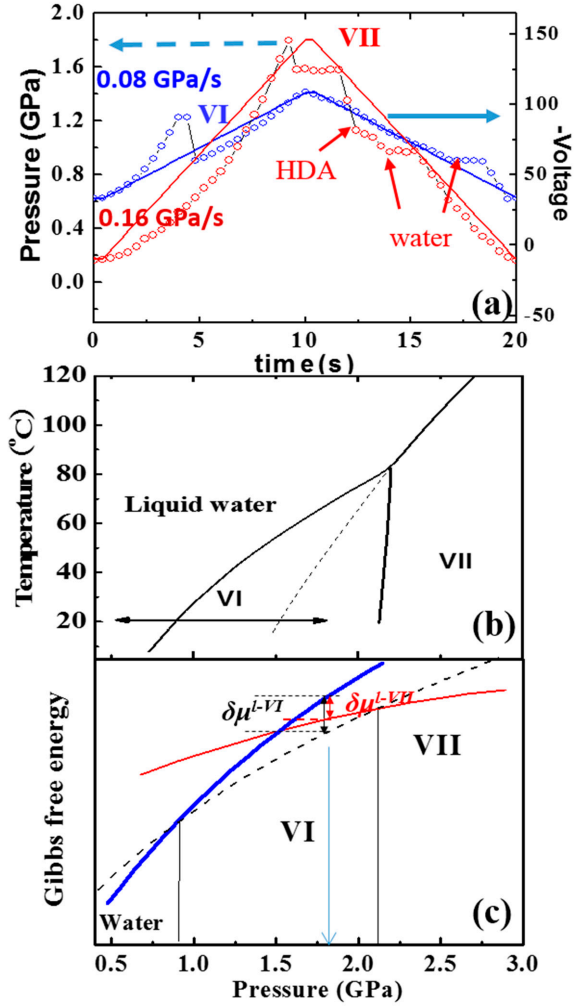

Figure 4. Pressure-time curves of H_2O by dynamic diamond anvil cell (dDAC) (**a**) [9]. Phase diagram of H_2O (**b**) and corresponding driving Gibbs free energy (**c**).

To understand the formation of the metastable ice VII phase, we consider the classical nucleation theory again. Figure 4c shows a smaller Gibbs free energy, $\delta\mu^{l\text{-}VII}$ (= $\Delta V^{l\text{-}VII}$ ΔP = 329 J/mol) for ice phase VII as compared to ice phase VI at 1.8 GPa ($\delta\mu^{l\text{-}VI}$ = 432 J/mol), in which the formation of ice VII phase is not allowed. And thus, the formation of the ice VII phase in ice phase VI pressure region implies that the nucleation barrier for the ice VII crystal is lower than for the ice phase VI crystal, due to its lower interfacial free energy. Using Equation (1), the interfacial free energies were estimated, in which the value for ice phase VII (22 mJ/mol) was indeed smaller than for ice phase VI (29 mJ/mol). Consequently, we can assign a smaller nucleation barrier (1.165 eV/atom) for ice phase VII than for ice phase VI (1.194 eV/atom) [9]. In a microscopic viewpoint, the formation of the metastable ice phase VII phase from over-pressurized water in the stable ice phase VI region can be understood by local structure similarity between high density water having BCC-like local order [61] and ice phase VII (BCC), rather than that of ice phase VI (tetragonal structure) [9].

3. Summary

One can often observe that metastable crystals form in the range of stable crystals. In this paper, three examples are reviewed, which show the formation of metastable crystals from metastable liquids in Ti-Zr-Ni metallic alloy liquids, an aqueous KDP solution, and liquid water. The metastable liquids are prepared by supercooling, supersaturating, and supercompressing using electrostatic levitation and dDAC techniques. In our finding, the formation of metastable crystals are attributed to the fact that the similarity in local structural orders between liquids and metastable crystals is considerably greater than that between liquids and stable crystals. Such structural similarity results in a smaller interfacial free energy that compensates for the smaller driving force and ultimately lowers the nucleation barrier for the metastable crystals. While our present work here provides a valuable insight for understanding multiple pathways of nucleation, more elaborate study is required for revealing the evolution of local orders in the metastable liquids. This new information could open more possibilities for finding new phenomena and materials.

Acknowledgments: The author would like to thank to S. Lee, Y. H. Lee, K. F. Kelton, and B. Lee for fruitful discussions and comments.

Conflicts of Interest: The author declares no conflict of interest.

References

1. Ostwald, W. Studien über die bildung und umwandlung fester körper. *Z. Phys. Chem.* **1897**, *22*, 289–330. [CrossRef]
2. Van Santen, R.A. The ostwald step rule. *J. Phys. Chem.* **1984**, *88*, 5768–5769. [CrossRef]
3. Vekilov, V.G. Phase diagrams and kinetics of phase transitions in protein solutions. *J. Phys.: Condens. Matter* **2012**, *24*, 193101. [CrossRef] [PubMed]
4. Lee, S.; Wi, H.S.; Jo, W.; Cho, Y.C.; Lee, H.H.; Jeong, S.-Y.; Kim, Y.-I.; Lee, G.W. Multiple pathways of crystal nucleation in an extremely supersaturated aqueous potassium dihydrogen phosphate (KDP) solution droplet. *Proc. Natl. Acad. Sci. USA* **2016**, *113*, 13618–13623. [CrossRef] [PubMed]
5. Gebauer, D.; Völkel, A.; Cölfen, H. Stable prenucleation calcium carbonate clusters. *Science* **2008**, *322*, 1819–1822. [CrossRef] [PubMed]
6. Baumgartner, J.; Dey, A.; Bomans, P.H.H.; Coadou, C.L.; Fratzl, P.; Sommerdijk, N.A.J.M.; Faivre, D. Nucleation and growth of magnetite from solution. *Nat. Mater.* **2013**, *12*, 310–314. [CrossRef] [PubMed]
7. Kelton, K.F.; Lee, G.W.; Gangopadhyay, A.K.; Croat, T.K.; Rathz, T.J.; Hyers, R.W.; Rogers, J.R.; Robinson, M.B.; Robinson, D.S. First X-ray scattering studies on electrostatically levitated metallic liquids: Demonstrated influence of local icosahedral order on the nucleation barrier. *Phys. Rev. Lett.* **2003**, *90*, 195504. [CrossRef] [PubMed]
8. Lee, G.W.; Cho, Y.C.; Lee, B.; Kelton, K.F. Interfacial free energy and medium range order: Proof of an inverse of Frank's hypothesis. *Phys. Rev. B* **2017**, *95*, 054202. [CrossRef]

9. Lee, G.W.; Evans, W.J.; Yoo, C.S. Crystallization of water in a dynamic diamond-anvil cell: Evidence for ice VII-like local order in supercompressed water. *Phys. Rev. B* **2006**, *74*, 134112. [CrossRef]
10. Chen, J.-Y.; Yoo, C.-S. High density amorphous ice at room temperature. *Proc. Natl. Acad. Sci. USA* **2011**, *108*, 7685–7688. [CrossRef] [PubMed]
11. Chung, S.-Y.; Kim, Y.-M.; Kim, J.-G.; Kim, Y.-J. Multiphase transformation and Ostwald's rule of stages during crystallization of a metal phosphate. *Nat. Phys.* **2009**, *5*, 68–73. [CrossRef]
12. Cahn, J.W. On spinodal decomposition. *Acta Metall.* **1961**, *9*, 795. [CrossRef]
13. Turnbull, D.; Cech, R.E. Formation of crystal nuclei in liquid metals. *J. Appl. Phys.* **1950**, *21*, 804. [CrossRef]
14. Waseda, Y. *The Structure of Non-Crystalline Materials*; McGraw-Hill Inc.: Pennsylvania Plaza, NY, USA, 1980.
15. Frank, F.C. Supercooling of liquids. *Proc. R. Soc. London A* **1952**, *215*, 43. [CrossRef]
16. Spaepen, F. *Solid State Physics*; Ehrenreich, H., Turnbull, D., Eds.; Academic Press: Boston, MA, USA, 1994; Volume 47, p. 1.
17. Spaepen, F.; Meyer, R. The surface tension in a structural model for the solid-liquid interface. *Scr. Metall.* **1976**, *10*, 257. [CrossRef]
18. Spaepen, F. A structural model for the solid-liquid interface in monatomic systems. *Acta Metall.* **1975**, *23*, 729. [CrossRef]
19. Murty, B.S.; Ping, D.H.; Hono, K. Nanoquasicrystallization of binary Zr–Pd metallic glasses. *Appl. Phys. Lett.* **2000**, *77*, 1102. [CrossRef]
20. Köster, U.; Meinhardt, J.; Roos, S.; Liebertz, H. Formation of quasicrystals in bulk glass forming Zr-Cu-Ni-Al alloys. *Appl. Phys. Lett.* **1996**, *69*, 179. [CrossRef]
21. Lee, G.W.; Gangopadhyay, A.K.; Croat, T.K.; Rathz, T.J.; Hyers, R.W.; Rogers, J.R.; Kelton, K.F. Link between liquid structure and the nucleation barrier for icosahedral quasicrystal, polytetrahedral, and simple crystalline phases in Ti-Zr-Ni alloys; verification of Frank's hypothesis. *Phys. Rev. B* **2005**, *72*, 174107. [CrossRef]
22. Notthoff, C.; Feuerbacher, B.; Franz, H.; Herlach, D.M.; Holland-Moritz, D. Direct determination of metastable phase diagram by synchrotron radiation experiments on undercooled metallic melt. *Phys. Rev. Lett.* **2011**, *86*, 1038–1041. [CrossRef] [PubMed]
23. Lee, G.W.; Gangopadhyay, A.K.; Kelton, K.F.; Hyers, R.W.; Rathz, T.J.; Rogers, J.R.; Robinson, D.S. Difference in icosahedral short-range order in early and late transition metal liquids. *Phys. Rev. Lett.* **2004**, *93*, 037802. [CrossRef] [PubMed]
24. Lee, G.W.; Jeon, S.; Park, C.; Kang, D.-H. Crystal–liquid interfacial free energy and thermophysical properties of pure liquid Ti using electrostatic levitation: Hypercooling limit, specific heat, total hemispherical emissivity, density, and interfacial free energy. *J. Chem. Thermodyn.* **2013**, *63*, 1. [CrossRef]
25. Lee, G.W.; Jeon, S.; Kang, D.H. Crystal–liquid interfacial free energy of supercooled liquid Fe using a containerless technique. *Cryst. Growth Des.* **2013**, *13*, 1786–1792. [CrossRef]
26. Jeon, S.; Kang, D.H.; Kang, S.H.; Kang, S.E.; Okada, J.T.; Ishikawa, T.; Lee, S.; Lee, G.W. Non-contact measurement of thermophysical properties of Fe, Fe-C, and Fe-C-Mn alloys in solid, supercooled, and stable liquid phases. *ISIJ Int.* **2016**, *56*, 719–722. [CrossRef]
27. Kang, D.-H.; Jeon, S.; Yoo, H.; Ishikawa, T.; Okada, J.T.; Paradis, P.-F.; Lee, G.W. Nanosized nucleus-supercooled liquid interfacial free energy and thermophysical properties of early and late transition liquid metals. *Cryst. Growth Des.* **2014**, *14*, 1103. [CrossRef]
28. Schenk, T.; Holland-Moritz, D.; Simonet, V.; Bellissent, R.; Herlach, D.M. Icosahedral short-range order in deeply undercooled metallic melts. *Phys. Rev. Lett.* **2002**, *89*, 075507. [CrossRef] [PubMed]
29. Lee, G.W.; Gangopadhyay, A.K.; Hyers, R.W.; Rathz, T.J.; Rogers, J.R.; Robinson, D.S.; Goldman, A.I.; Kelton, K.F. Local structure of equilibrium and supercooled Ti-Zr-Ni liquids. *Phys. Rev. B* **2008**, *77*, 184102. [CrossRef]
30. Kim, T.H.; Lee, G.W.; Gangopadhyay, A.K.; Hyers, R.W.; Rogers, J.R.; Goldman, A.I.; Kelton, K.F. Structural studies of a Ti-Zr-Ni quasicrystal-forming liquid. *J. Phys.: Conden. Matt.* **2007**, *19*, 455212. [CrossRef]
31. Kim, T.H.; Gangopadhyay, A.K.; Xing, L.Q.; Lee, G.W.; Shen, Y.T.; Kelton, K.F.; Goldman, A.I.; Hyers, R.W.; Rogers, J.R. Role of Ti in the formation of Zr-Ti-Cu-Ni-Al glasses. *Appl. Phys. Lett.* **2005**, *87*, 251924. [CrossRef]
32. Herlach, D.M.; Gao, J.; Volkmann, T. Nucleation and phase-selection in undercooled melts. *Mater. Sci. Eng. A* **2004**, *375–377*, 9–15. [CrossRef]

33. Lee, G.W.; Gangopadhyay, A.K.; Kelton, K.F. Effect of microalloying on the formation and stability of the Ti-Zr-Ni icosahedral quasicrystal. *J. Alloy Compd.* **2012**, *537*, 171–174. [CrossRef]
34. Lee, S.; Jo, W.; Cho, Y.C.; Lee, H.H.; Lee, G.W. Solution electrostatic levitator for measuring surface properties and bulk structures of an extremely supersaturated solution drop above metastable zone width limit. *Rev. Sci. Instrum.* **2017**, *88*, 055101. [CrossRef] [PubMed]
35. Salzmann, C.G.; Kohl, I.; Loerting, T.; Mayer, E.; Hallbrucker, A. Pure ices IV and XII from high-density amorphous ice. *Can. J. Phys.* **2003**, *81*, 25. [CrossRef]
36. Koh, C.A. Towards a fundamental understanding of natural gas hydrates. *Chem. Soc. Rev.* **2002**, *31*, 157. [CrossRef] [PubMed]
37. Cavalleri, M.; Ogasawara, H.; Pettersson, L.G.M.; Nilsson, A. The interpretation of X-ray absorption spectra of water and ice. *Chem. Phys. Lett.* **2002**, *364*, 363. [CrossRef]
38. Loerting, T.; Winkel, K.; Seidl, M.; Bauer, M.; Mitterdorfer, C.; Handle, P.H.; Salzmann, C.G.; Mayer, E.; Finney, J.L.; Bowron, D.T. How many amorphous ices are there? *Phys. Chem. Chem. Phys.* **2011**, *13*, 8783. [CrossRef] [PubMed]
39. Mishima, O.; Calvert, L.D.; Whalley, E. 'Melting ice' I at 77 K and 10 kbar: A new method of making amorphous solids. *Nature* **1984**, *310*, 393. [CrossRef]
40. Loerting, T.; Salzman, C.; Kohl, I.; Meyer, E.; Hallbrucker, A. A second distinct structural "state" of high-density amorphous ice at 77 K and 1 bar. *Phys. Chem. Chem. Phys.* **2001**, *3*, 5355. [CrossRef]
41. Lee, G.W.; Evans, W.J.; Yoo, C.S. Dynamic pressure-induced dendritic and shock crystal growth of ice VI. *Proc. Natl. Acad. Sci. USA* **2007**, *104*, 9178–9181. [CrossRef] [PubMed]
42. Kelton, K.F. *Solid State Physics*; Ehrenreich, H., Turnbull, D., Eds.; Academic Press: Boston, MA, USA, 1991; p. 75.
43. Turnbull, D. Kinetics of solidification of supercooled liquid mercury droplets. *J. Chem. Phys.* **1952**, *20*, 411. [CrossRef]
44. Thompson, C.V.; Spaepen, F. On the approximation of the free energy change on crystallization. *Acta Metall.* **1979**, *27*, 1855. [CrossRef]
45. Battezzati, L.; Garonne, E. On the approximations of the free energy of undercooled glass-forming metallic melts. *Z. Metallk.* **1984**, *75*, 305.
46. Paradis, P.-F.; Ishikawa, T.; Lee, G.W.; Holland-Moritz, D.; Brillo, J.; Rhim, W.-K.; Okada, J.T. Materials properties measurements and particle beam interactions studies using electrostatic levitation. *Mater. Sci. Eng. R* **2014**, *76*, 1. [CrossRef]
47. Lee, G.W.; Gangopadhyay, A.K.; Kelton, K.F. Phase diagram studies of Ti-Zr-Ni alloys containing less than 40 at.% Ni and estimated critical cooling rate for icosahedral quasicrystal formation from the liquid. *Acta Mater.* **2011**, *59*, 4964–4973. [CrossRef]
48. Kang, D.H.; Zhang, H.; Yoo, H.; Lee, H.H.; Lee, S.; Lee, G.W.; Lou, H.; Wang, X.; Cao, Q.; Zhang, D.; et al. Interfacial free energy controlling glass-forming ability of Cu-Zr alloys. *Sci. Rep.* **2014**, *4*, 5167. [CrossRef] [PubMed]
49. Steinhardt, P.J. Solid-state physics: How does your quasicrystal grow? *Nature* **2008**, *452*, 43. [CrossRef] [PubMed]
50. Keys, A.S.; Glotzer, S.C. How do quasicrystals grow? *Phys. Rev. Lett.* **2007**, *99*, 235503. [CrossRef] [PubMed]
51. Liu, X.J.; Xu, Y.; Hui, X.; Lu, Z.P.; Li, F.; Chen, G.L.; Lu, J.; Liu, C.T. Metallic liquids and glasses: Atomic order and global packing. *Phys. Rev. Lett.* **2010**, *105*, 155501. [CrossRef] [PubMed]
52. Chen, J.; Lin, S.; Yang, F.; Wang, J.; Lang, J. Effect of alcoholic additives on the nucleation of KDP and DKDP crystals. *J. Cryst. Growth* **1997**, *179*, 226–230.
53. Wojciechowski, K.; Kibalczyc, W. Light scattering study of KH_2PO_4 and $BaSO_4$ nucleation process. *J. Cryst. Growth* **1986**, *76*, 379–382. [CrossRef]
54. Shanmungham, M.; Gnanam, F.D.; Ramasamy, P. Nucleation studies in supersaturated potassium dihydrogen orthophosphate solution and the effect of soluble impurities. *J. Mater. Sci.* **1984**, *19*, 2837–2844. [CrossRef]
55. Joshi, M.S.; Antony, A.V. Nucleation in supersaturated potassium dihydrogen orthophosphate solutions. *J. Cryst. Growth* **1979**, *46*, 7–9. [CrossRef]
56. Zaitseva, N.; Carman, L. Rapid growth of KDP-type crystals. *Prog. Cryst. Growth Charact. Mater.* **2001**, *43*, 1–118. [CrossRef]

57. Parikh, K.D.; Parekh, B.B.; Dave, D.J.; Joshi, M.J. Nucleation kinetics of L-arginine, L-lysine and L-alanine doped potassium dihydrogen phosphate crystals. *JCPT* **2013**, *3*, 92–96. [CrossRef]
58. Chernov, A.A. Secondary nucleation induced by the cracking of a growing crystal: KH2PO4 (KDP) and K(H,D)2PO4 (DKDP). *J. Cryst. Growth* **1990**, *102*, 793–800. [CrossRef]
59. Söhnel, O. Electrolyte crystal-aqueous solution interfacial tensions from crystallization data. *J. Cryst. Growth* **1982**, *57*, 101–108. [CrossRef]
60. Evans, W.J.; Yoo, C.S.; Lee, G.W.; Cynn, H.; Lipp, M.J.; Visbeck, K. Dynamic diamond anvil cell (dDAC): A novel device for studying the dynamic-pressure properties of materials. *Rev. Sci. Instrum.* **2007**, *78*, 073904. [CrossRef] [PubMed]
61. Saitta, A.M.; Datchi, F. Structure and phase diagram of high-density water: The role of interstitial molecules. *Phys. Rev. E* **2003**, *67*, 020201(R). [CrossRef] [PubMed]